Hindawi Publishing Corporation
EURASIP Journal on Advances in Signal Processing
Volume 2008, Article ID 347495, 16 pages
doi:10.1155/2008/347495

Research Article

Flicker Compensation for Archived Film Sequences Using a Segmentation-Based Nonlinear Model

Guillaume Forbin and Theodore Vlachos

Centre for Vision, Speech and Signal Processing, University of Surrey, GU2 7XH, Guildford, Surrey, UK

Correspondence should be addressed to Guillaume Forbin, g.forbin@surrey.ac.uk

Received 28 September 2007; Accepted 23 May 2008

Recommended by Bernard Besserer

A new approach for the compensation of temporal brightness variations (commonly referred to as flicker) in archived film sequences is presented. The proposed method uses fundamental principles of photographic image registration to provide adaptation to temporal and spatial variations of picture brightness. The main novelty of this work is the use of spatial segmentation to identify regions of homogeneous brightness for which reliable estimation of flicker parameters can be obtained. Additionally our scheme incorporates an efficient mechanism for the compensation of long duration film sequences while it addresses problems arising from varying scene motion and illumination using a novel motion-compensated grey-level tracing approach. We present experimental evidence which suggests that our method offers high levels of performance and compares favourably with competing state-of-the-art techniques.

1. INTRODUCTION

Flicker refers to random temporal fluctuations in image intensity and is one of the most commonly encountered artefacts in archived film. Inconsistent film exposure at the image acquisition stage is its main contributing cause. Other causes may include printing errors in film processing, film ageing, multiple copying, mould, and dust.

Film flicker is immediately recognisable even by nonexpert viewers as a signature artefact of old film sequences. Its perceptual impact can be significant as it interferes substantially with the viewing experience and has the potential of concealing essential details. In addition it can be quite unsettling to the viewer, especially in cases where film is displayed simultaneously with video or with electronically generated graphics and captions as is typically the case in modern-day television documentaries. It may also lead to considerable discomfort and eye fatigue after prolonged viewing. Camera and scene motion can partly mask film flicker and as a consequence, the latter is much more noticeable in sequences consisting primarily of still frames or frames with low-motion content. In addition it must also be pointed out that inconsistent intensity between successive frames reduces motion estimation accuracy and by consequence the efficiency of compression algorithms.

Flicker has often been categorised as a global artefact in the sense that it usually affects all the frames of a sequence in their entirety as opposed to so-called local artefacts such as dirt, dust, or scratches which affect a limited number of frames and are usually localised on the image plane. Nevertheless it is by no means constant within the boundaries of a single frame as explained in the next section and one of the main aims of this work is to address this issue.

1.1. Spatial variability

Flicker can be spatially variable and can manifest itself in any one of the following ways. Firstly, when flicker affects approximately the same position of all the frames in a sequence. This may occur directly during film shooting if scene lighting is not synchronised with the shutter of the camera. For example, if part of the scene is illuminated with synchronised light while the rest is illuminated with natural light a localised flickering effect may occur. This can also be due to *fogging* (dark areas in the film strip) which is caused

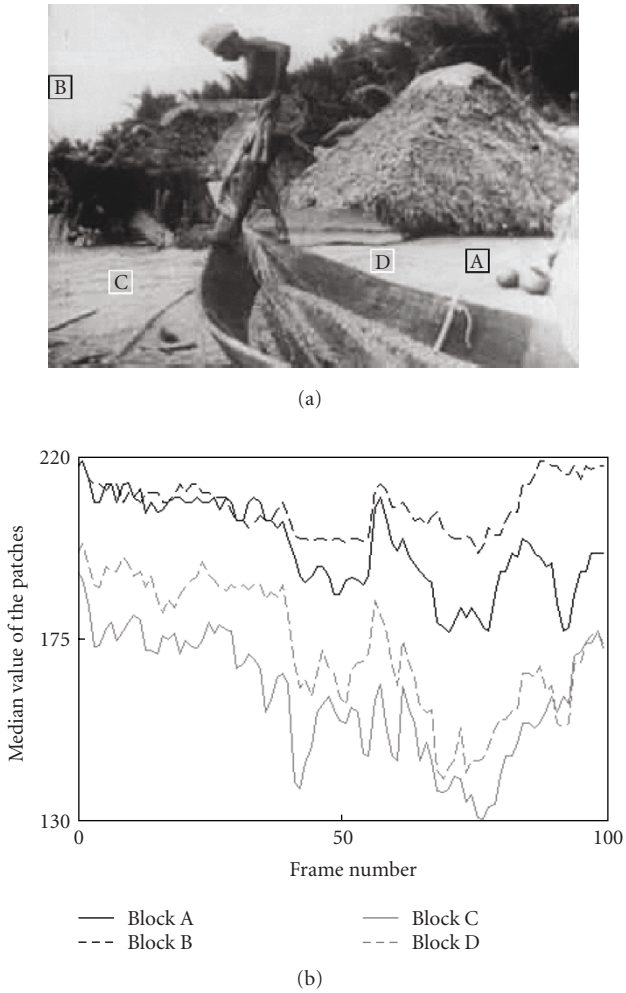

FIGURE 1: (a) Test sequence *Boat* used to illustrate spatial variability of flicker measured at selected location. (b) Evolution of the median intensity of the selected blocks.

by the accidental exposure of film to incident light, partial immersion or the use of old or spent chemicals on the film strip in the developer bath. Drying stains from chemical agents can also generate flicker [1–6].

It is also possible that flicker localisation varies randomly. This is the case when the film strip ages badly and becomes affected by mould, or when it has been charged with static charge generated from mechanical friction. The return to a normal state often produces static marks.

Figure 1 shows the first frame of the test sequence *Boat* (*Our Shrinking World* (1946) - Young America Films, Inc. - Sd, B&W. (1946)). The camera lingers in the same position during the 93 frames of the sequence. There is also some slight unsteadiness. Despite some local scene motion, overall motion content is low. This sequence is chosen to illustrate that the spatial variation of flicker is not perceivable on the top-left part of the shot, while the bottom-left part changes from brighter initially to darker later on. On the right-hand side of the image, flicker is more noticeable, with faster variations of higher amplitude. This is shown in Figure 1, where the median intensities of four manually selected blocks (16×16 pixels) located at different parts of the frame are plotted as a function of frame number.

The selected blocks are motionless, low-textured and have pairwise similar grey levels (A, B and C, D) at the start of the sequence. As the sequence evolves we can clearly observe that each block of a given pair undergoes a substantially different level of flicker with respect to the other block. This example also illustrates that flicker can affect only a temporal segment of a sequence. Indeed, from the beginning of the shot to frame 40 the evolution of the median intensities for blocks A and B is highly similar, thus degradation is low compared to the segment that follows the first 40 frames.

This paper introduces two novel concepts for flicker compensation. Firstly, the estimation of the flicker compensation profile is performed on regions of homogeneous intensity (Section 4). The incorporation of segmentation information enhances the accuracy and the robustness of flicker estimation.

Secondly, the concept of grey-level tracing (developed in Section 5) is a fundamental mechanism for the correct estimation of flicker parameters as they evolve over time. Further, this is integrated into a motion-compensated, spatially-adaptive algorithm which also incorporates the nonlinear modelling principles proposed in [7, 8]. It is worth noting that [7] is a proof-of-concept algorithm that was originally designed to compensate frame pairs but was never engineered as a complete solution for long-duration sequences containing arbitrary camera and scene motion, intentional scene illumination changes, and spatially varying flicker effects.

This is demonstrated in Figure 2 where the algorithm in [7] achieves flicker removal by stabilising the global frame intensity over time but only with respect to the first frame of the sequence which is used as a reference. In contrast the proposed algorithm is well-equipped to deal with motion, intentional illumination fluctuations and spatial variations and, together with a shot change detector, it can be used as a complete solution for any sequence irrespective of content and length.

This paper is organised as follows. Section 2 reviews the literature of flicker compensation while Section 3 provides an overview of our previous baseline approach based on a nonlinear model and proposed in [7]. Improvements reported in [8] and related to the flicker compensation profile estimation are presented in Sections 3.2 and 3.3. Spatial adaptation and incorporation of segmentation information are described in Section 4. Finally, a temporal compensation framework using a motion-compensated grey-level tracing approach is presented in Section 5 and experimental results are presented in Section 6. Conclusions are drawn in Section 7.

2. LITERATURE REVIEW

Flicker compensation techniques broadly fall into two categories. Initial research addressed flicker correction as a global compensation in the sense that an entire frame is corrected in a uniform manner without taking into account the spatial

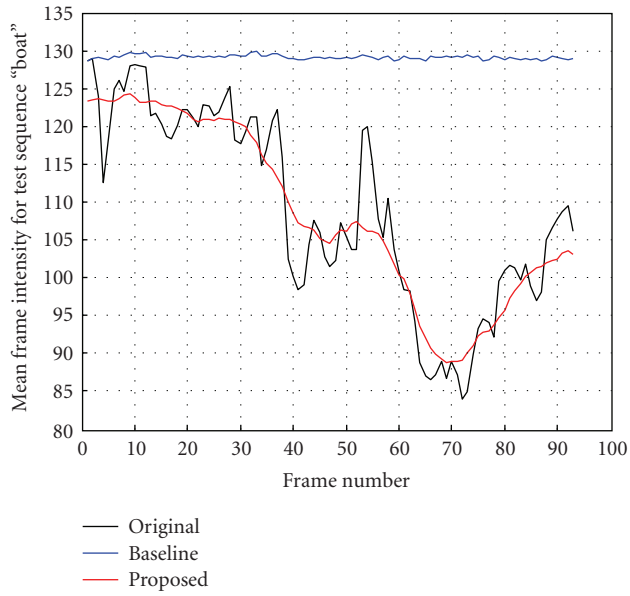

FIGURE 2: Comparison of mean frame intensity as a function of time between the original, the baseline scheme [7, 8] and the proposed approach.

variability issues illustrated previously. More recent attempts have addressed spatial variability.

2.1. Global compensation

Previous research has frequently led to linear models where the corrected frame was obtained by linear transformation of the original pixel values. A global model was formulated which assumed that the entire degraded frame was affected with a constant intensity offset. In [1], flicker was modelled as a global intensity shift between a degraded frame and the mean level of the shot to which this frame belongs. In [2], flicker was modelled as a multiplicative constant relating the mean level of a degraded frame to a reference frame. Both the additive and multiplicative models mentioned above require the estimation of a single parameter which although straightforward fails to account for spatial variability.

In [3] it was observed that archive material typically has a limited dynamic range. Histogram stretching was applied to individual frames allowing the available dynamic range to be used in its entirety (typically $[0 : 255]$ for 8 bits per pixel image). Despite the general improvement in picture quality the authors admitted that this technique was only moderately effective as significant residual intensity variations remained. The concept of histogram manipulation has been further explored in [1] where degradation due to flicker was modelled as a linear two-parameters grey-level transformation. The required parameters were estimated under the constraint that the dynamic range of the corresponding non-degraded frames does not change with time.

Work in [4, 9] approached the problem using histogram equalisation. A degraded frame was first histogram-equalised and then inverse-histogram was performed with respect to a reference frame. Inverse equalisation was carried out in order for the degraded frame to inherit the histogram profile of the reference. Our previous work described in [7] used non-linear compensation motivated by principles of photographic image registration. Its main features are summarised in Section 3.1. Table 1 presents a brief overview of global compensation methods.

2.2. Spatially-adaptive compensation

Recent work has considered the incorporation of spatial variability into the previous models. In [5] a semi-global compensation was performed based on a block-partitioning of the degraded frame. Each block was assumed to have undergone a linear intensity transformation independent of all other blocks. A linear minimum mean-square error (LMMSE) estimator was used to obtain an estimate of the required parameters. A block-based motion detector was also used to prevent blocks containing motion to contribute to the estimation process and thus the missing parameters due to the motion were interpolated using a successive over-relaxation technique. This smooth block-based sparse parameter field was bi-linearly interpolated to yield a dense pixel-accurate correction field.

Research carried out in [10, 11] has extended the global compensation methods of [1, 2] by replacing the additive and multiplicative constants with two-dimensional second-order polynomials. It matches the visual impression one gets by inspecting actual flicker-impaired material. In [10] a robust hierarchical framework was proposed to estimate the polynomial functions, ranging from zero-order to second-order polynomials. Parameters were obtained using M-estimators minimising a robust energy criterion while lower-order parameters were used as an initialisation for higher-order ones. Nevertheless, it has to be pointed out that the previous estimators were integrated in a linear regression scheme, which introduces a bias if the frames are not entirely correlated (regression "fallacy" or regression "trap" [12], demonstrated by Galton [13]). In [11] an alternative approach to the parameter estimation problem which tried to solve this issue was proposed. A histogram-based method [6] was formulated later on and joint probability density functions (pdfs) (establishing a correspondence between grey levels of consecutive frames) were estimated locally in several control points using a maximum-a-posteriori (MAP) technique. Afterwards a dense correction function was obtained using interpolation splines. The same authors proposed recently in [14] a flicker model able to deal within a common framework with very localised and smooth spatial variations. Flicker model is parametrised with a single parameter per pixel and is able to handle non-linear distorations. A so-called "mixing model" is estimated reflecting both the global illumination of the scene and the flicker impact.

A method suitable for motionless sequences was described in [15]. It was based on spatiotemporal segmentation, the main idea being the isolation of a common background for the sequence and the moving objects. The background was estimated through a regularised average

Table 1: An overview of the global flicker compensation techniques.

Global compensation techniques	Summary
Wu and Suter [1]	*linear compensation*—flicker is modelled as a global intensity shift.
Decencière [2]	*linear compensation*—flicker is modelled as a multiplicative constant.
Richardson and Suter [3]	*histogram-based compensation*—histogram stretching across the available greyscale.
Wu and Suter [1]	*histogram-based compensation*—histogram stretching across the reference frame greyscale.
Schallauer et al. [9] and Naranjo and Albiol [4]	*histogram-based compensation*—histogram equalisation with respect to a reference frame.
Vlachos [7]	*Non-linear approach*: flicker parameters are estimated independently for each grey-level and a compensation profile is obtained.

Table 2: An overview of the spatially adaptive compensation techniques.

Spatially adaptive compensation techniques	Summary
van Roosmalen et al. [5]	*Linear compensation*: block-partitioning of the degraded frame. Smoothing of the sparse parameter field.
Ohuchi et al. [10]	*Linear compensation*: flicker is modelled as 2-parameter 2nd order polynomials, hierarchical parameters estimation.
Kokaram et al. [11]	*Linear compensation*: flicker is modelled as 2-parameter 2nd order polynomials, parameters estimation based on an unbias linear regression.
Jung et al. [15]	*Linear compensation*: spatio-temporal segmentation isolating the background and the moving objects. Temporal average of the grey levels preserving the edges to reduce the flicker.
Pitié et al. [6]	*Histogram-based compensation*: Joint probability density functions (pdfs) estimated locally in several control points. Dense correction function obtained using interpolation splines.
Forbin et al. [8]	*Non-linear formulation*: block-partionning of the degraded frame and estimation of intensity error profiles on each blocks using motion-compensated frame. Non-linear Interpolation of the compensation values weighted by estimated reliabilities.
Pitié et al. [14]	*Pixel-based flicker estimation*: flicker strength is estimated for each pixel using a "mixing model" of the global illumination.

(preserving the edges) of the sequence frames, while moving objects were motion compensated, averaged and regularised to preserve spatial continuities. Table 2 presents a brief overview of the above methods.

Based on the nonlinear model formulated in [7], we proposed significant enhancement towards a motion-compensation-based spatially-adaptive model [8]. These improvements are extensively detailed in Sections 3.2, 3.3, and 4.1.

2.3. Compensation for sequences of longer duration

While the above efforts addressed the fundamental estimation problem with varying degrees of success far fewer attempts were made to formulate a complete and integrated compensation framework suitable for the challenges posed by processing longer sequences. In such sequences the main challenges relate to continuously evolving scene motion and illumination rendering considerably more difficult the appointment of reference frames. In [9] reference frames were appointed and a linear combination of the inverse histogram equalisation functions of the two closest reference frames (forward/backward) was used for the compensation. In [4] a target histogram was calculated for histogram equalisation purposes by averaging neighbouring frames' histograms within a sliding window. This technique was also used in [16], but there the target histogram was defined as a weighted intermediary between the current frame and its neighbouring histograms, the computation being inspired from scale-time equalisation theory.

In [5] compensation was performed recursively. Error propagation is likely in this framework as previously generated corrections were used to estimate future flicker parameters. A bias was introduced and the restored frame was a mixture of the actual compensated frame and the original degraded one. In [11, 14] an approach motivated by video stabilisation described in [2] is proposed. Several flicker parameter estimations are computed for a degraded

frame within a temporal window and an averaging filter is employed to provide a degree of smoothing of those parameters.

3. NONLINEAR MODELLING

This section summarises our previous work reported in [7], which addressed the problem using photographic acquisition principles leading to a nonlinear intensity error profile between a reference and degraded frame. The proposed model assumes that flicker is originated from exposure inconsistencies at the acquisition stage. Quadratic and cubic models are provided, which means that the method is able to compensate for other sources of flicker respecting these constraints. Important improvements are discussed in Sections 3.2 and 3.3.

3.1. Intensity error profile estimation based on the Density versus log-Exposure characteristic

The Density versus log-Exposure characteristic $D(\log E)$ attributed to Hurter and Driffield [17] (Figure 3) is used to characterise exposure inconsistencies and their associated density errors.

The slope of the linear region is often referred to as gamma and defines the contrast characteristics of the photosensitive material used for image acquisition. In [7] it was shown that an observed image intensity I with underlying density D and associated errors ΔI and ΔD due to flicker are related via

$$I \longrightarrow \Delta I, \tag{1}$$

which can as well be expressed by

$$\exp(-D) \longrightarrow \Delta D \cdot \exp(-D). \tag{2}$$

The mapping $I \rightarrow \Delta I$ relates grey-level I in the reference image and the intensity error ΔI in the degraded image. In other words, this mapping determines the amount of correction ΔI to be applied to a particular grey-level I in order to undo the flicker error. As the Hurter-Driffield characteristic is usually film stock dependent and hence unknown, D and ΔD are difficult to obtain. Nevertheless an intensity error profile ΔI across the entire greyscale can be estimated numerically. Figure 3 shows a typical such profile which is highly non-linear, concave, peaking at the midgrey region and decreasing at the extremes of the available scale, as plotted in Figure 4. As a consequence, a quadratic polynomial could be chosen to approximate the intensity error profile in a parametrised fashion. Nevertheless, telecine grading (contrast, greyscale linearity, and dynamic range adjustments performed during film-to-video transfer) can introduce further non-linearity as discussed in [7] and a cubic polynomial approximation is more appropriate in those cases.

An intensity error profile $\Delta I_{t,\text{ref}}$ is determined between a reference and a degraded frame F_{ref} and F_t, respectively, where I_{ref} and $I_t = I_{\text{ref}} - \Delta I_{t,\text{ref}}(I_t)$ are grey levels of co-sited pixels in the reference and degraded frames and $\Delta I_{t,\text{ref}}(I_t)$ is

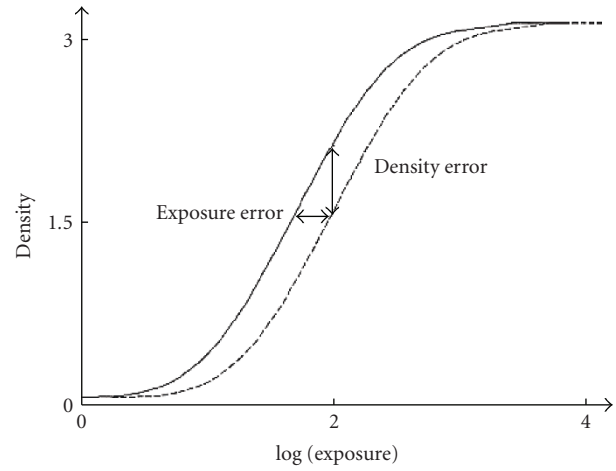

Figure 3: Hurter-Driffield $D(\log E)$ characteristic (dashed) and density error curve (solid) due to exposure inconsistencies.

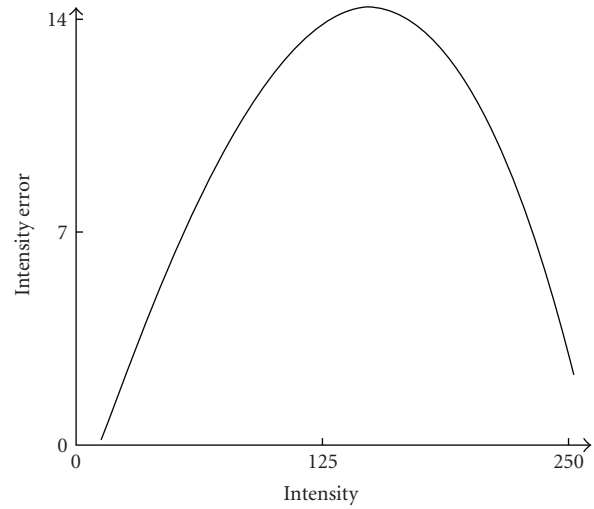

Figure 4: Theoretical intensity error profile as a function of intensity (all units are grey-levels).

the flicker component for grey-level I_t. For monochrome 8-bits-per-pixel images, $I_t, I_{\text{ref}} \in \{0, 1, \ldots, 255\}$. This compensation profile allows to reduce F_t flicker artefact according to F_{ref}. In this framework, F_{ref} is chosen arbitrarily, as a nondegraded frame is usually not available. It is assumed that motion content between those two images is low and does not interfere in the calculations. To estimate $\Delta I_{t,\text{ref}}(I_t)$, pixel differences between all pixels with intensity I_t in the degraded frame and their cosited pixels in position $\vec{p} = (x, y)$ in the reference frame are computed and a histogram $H_{t,\text{ref}}(I_t)$ of the error is compiled as follows:

$$\forall F_t(\vec{p}) = I_t : H_{t,\text{ref}}(I_t) = \text{hist}\left(F_t(\vec{p}) - F_{\text{ref}}(\vec{p})\right). \tag{3}$$

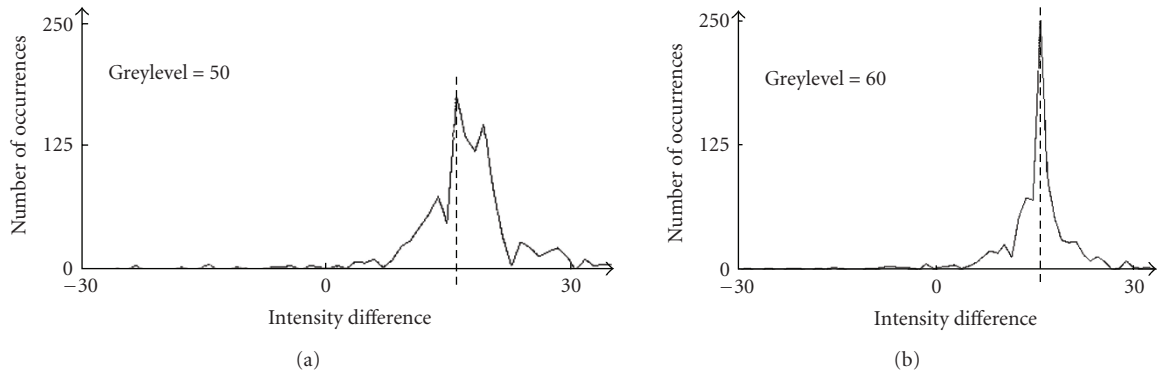

Figure 5: Intensity difference histograms $H_{t,\text{ref}}(50)$ and $H_{t,\text{ref}}(60)$ and their maxima for two consecutive frames of test sequence *Caption*.

An example is shown in Figure 5 for the test sequence *Caption* and two sample grey levels. The intensity error is given by

$$\Delta I_{t,\text{ref}}(I_t) = \arg\max\{H_{t,\text{ref}}(I_t)\}. \tag{4}$$

The process is repeated for each intensity level I_t to compile an intensity error profile for the entire greyscale. As the above computation is obtained from real images, the profile $\Delta I_{t,\text{ref}}$ is unlikely to be smooth and is likely to contain noisy measurements. Either a quadratic or cubic polynomial least-squares fitting can be applied to the compensation profile. Cubic approximation is more complex and more sensitive to noise but is able to cope with nonlinearity originated from telecine grading, as discussed in [7]:

$$\vec{A} = \arg\min \sum_{I_t} \left(P_{t,\text{ref}}(I_t) - \Delta I_{t,\text{ref}}(I_t)\right)^2,$$
$$\text{with } \vec{A} = \{a_0, \ldots, a_L\}, \quad P_{t,\text{ref}}(I_t) = \sum_{k=0}^{L} a_k \cdot I_t^k. \tag{5}$$

L being the polynomial order. An example is shown in Figure 4. Finally the correction applied to the pixel at location $\vec{p}$ is:

$$F_t'(\vec{p}) = F_t(\vec{p}) + P_{t,\text{ref}}(F_t(\vec{p})). \tag{6}$$

3.2. Grey-level intensity error reliability weighting

The first important improvement to the baseline scheme in [7] is motivated by the observation that taking into account the frequency of occurrence of grey-levels can enhance the reliability of the estimation process. This enhancement is presented in [8]. grey-levels with low pixel representation should be less relied upon and vice versa. In addition, $\Delta I_{t,\text{ref}}$ estimation accuracy can vary for different intensities as illustrated in Figure 5. It can be seen for example that $H_{t,\text{ref}}(50)$ is spread around an intensity error of 15 and even if the maximum is reached for 12, many pixels actually voted for a different compensation value. On the other hand the strength of consensus (i.e., height of the maximum) of $H_{t,\text{ref}}(60)$ suggests a more unanimous verdict. Thus the reliability of $\Delta I_{t,\text{ref}}$ depends on the frequency of I_{ref} but also on $H_{t,\text{ref}}$. A weighted polynomial least square fitting [18] is then used to compute the intensity error profile and the weighting function reflecting grey-level reliability is chosen as:

$$r_{t,\text{ref}}(I_t) = \max\{H_{t,\text{ref}}(I_t)\}. \tag{7}$$

Indeed, if I_t does not occur very frequently in F_t then $r_{t,\text{ref}}(I_t)$ will be close to 0 and reliability will be influenced accordingly. The polynomial $C_{t,\text{ref}}$ parameters are now obtained as the solution to the following weighted least-squares minimisation problem:

$$\vec{A}' = \arg\min \sum_{I_t} r_{t,\text{ref}}(I_t) \cdot \left(C_{t,\text{ref}}(I_t) - \Delta I_{t,\text{ref}}(I_t)\right)^2. \tag{8}$$

An example of reliability distribution $r_{t,\text{ref}}$ is shown at the bottom of Figure 6, and highlights that pixel intensities above 140 are poorly represented. A comparison between the resulting unweighted correction profile $P_{t,\text{ref}}$ (dashed line) and the improved one $C_{t,\text{ref}}$ (solid line) confirms that more densely populated grey-levels have a stronger influence on the fidelity of the fitted profile.

A side benefit of this enhancement is that it allows our scheme to deal with compressed sequences such as MPEG material. The quantisation used in compression may obliterate certain grey levels. An absent grey-level I_t implies that $H_{t,\text{ref}}(I_t) = 0$, thus $r_{t,\text{ref}}(I_t) = 0$, which means that $\Delta I_{t,\text{ref}}(I_t)$ will not be used at all in the fitting process.

3.3. Motion compensated intensity error profile estimation

The above works well if motion variations between a reference and a degraded frame are low. As stated in [8], motion compensation must be employed to be able to cope with longer duration sequences. This will enable the estimation of a flicker compensation profile between a degraded- and a motion-compensated reference frame $F_{t,\text{ref}}^c$. In our work we use the well-known Black and Anandan dense motion estimator [19] as it is well equipped to deal with the violation

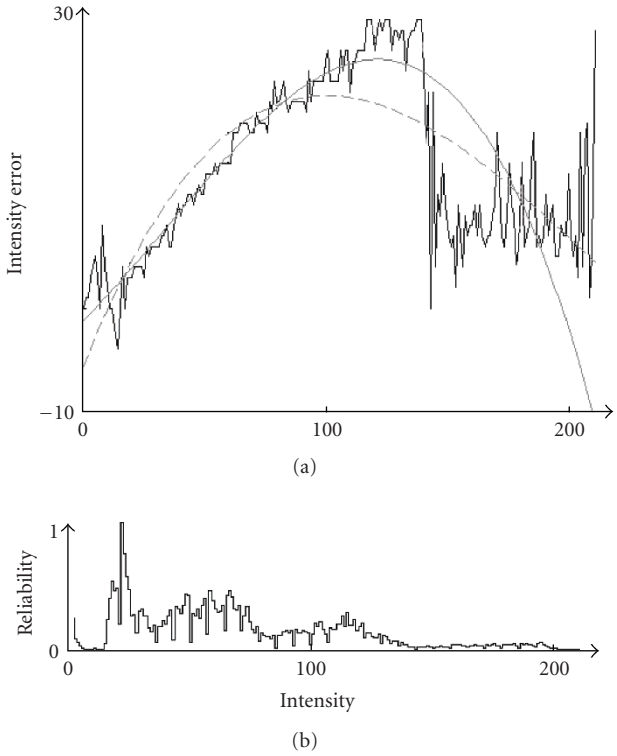

Figure 6: Measured and polynomial approximated (dashed:basic fitting - solid:weighted fitting) intensity error profiles as a function of intensity between the first two frames of test sequence *Caption*. A quadratic model is used. The histogram below shows the normalised confidence values $r_{t,\text{ref}}$ for each grey-level.

of the brightness constancy assumption, which is a defining feature of flicker applications. Other dense or sparse motion estimators can be used depending of robustness and speed requirements. Robustness is crucial as incorrect motion estimation will fail the flicker compensation. The motion compensation error will provide a key influence towards intensity error profile estimation. Indeed, (3) attributes the same importance to each pixel contributing to the histogram. The motion compensation error is employed to decrease the influence of poorly compensated pixels. This is achieved by compiling $H^c_{t,\text{ref}}(I_t)$ using real-valued (as opposed to unity) increments for each pixel located at $\vec{p}$ (i.e., $F_t(\vec{p}) = I_t$) according to the following relationship:

$$e^c_{t,\text{ref}}(\vec{p}) = 1 - \frac{|E^c_{t,\text{ref}}(\vec{p})|}{\max\{|E^c_{t,\text{ref}}(\vec{p})|\}}, \tag{9}$$

$E^c_{t,\text{ref}}$ being the motion prediction error, that is, $E^c_{t,\text{ref}} = F^c_{\text{ref}} - F_t$. Thus $e^c_{t,\text{ref}}(\vec{p})$ varies between 0 and 1 and is inversely proportional to $E^c_{t,\text{ref}}(\vec{p})$, and so high confidence is placed on pixels with a low motion compensation error and vice versa. In other words, areas where local motion can be reliably predicted (hence yielding low levels of motion compensation error) are allowed to exert high influence on the estimation of flicker parameters. Pixels with poorly estimated motion, on the other hand, are prevented from contributing to the flicker correction process.

4. SPATIAL ADAPTATION

The above compensation scheme performs well if the degraded sequence is globally affected by flicker artefact. However, as illustrated in Section 1.1 this is not always the case. Spatial adaptation is achieved by taking into account regions of homogeneous intensity. The incorporation of segmentation information enhances the accuracy and the robustness of flicker parameters estimation.

4.1. Block-based spatial adaptation

Spatial adaptation requires mixed block-based/region-based frame partitioning. The block-based part is illustrated in Figure 7. Correction profiles $C_{t,\text{ref},b}$ are computed independently for each block b of frame F_t. As brute force correction of each block would lead to blocking artefacts at block boundaries (Figure 8), a weighted bilinear interpolation is used.

It is assumed initially that flicker is spatially invariant within each block. For each block a correction profile is computed independently between I_{ref} and I_t, yielding values for $\Delta I_{t,\text{ref},b}$, $C_{t,\text{ref},b}$ and $r_{t,\text{ref},b}$, $b = [1;B]$, b being the block index and B the total number of blocks.

Blocking is avoided by applying bilinear interpolation of the B available correction values $C_{t,\text{ref},b}(F_t(\vec{p}))$ for pixel $\vec{p}$. Interpolation is based on the inverse of the Euclidean distance $c_b(\vec{p}) = \sqrt{(x - x_b)^2 + (y - y_b)^2}$,

$$d_b(\vec{p}) = \frac{1}{c_b(\vec{p}) + 1} \tag{10}$$

with (x_b, y_b) being the coordinates of the centre of the block b for which the block-based correction derived earlier is assumed to hold true.

This interpolation smooths the transitions across blocks boundaries. In addition, reliability measurements $r_{t,\text{ref},b}$ of $C_{t,\text{ref},b}$ detailed in Section 3.2 are also used as a second weight in the bilinear interpolation. This allows to discard measurements coming from blocks where $F_t(\vec{p})$ is poorly represented. Polynomial approximation on blocks with a low grey-level dynamic will only be accurate on a narrow part of the greyscale, but rather unpredictable for absent grey levels. $r_{t,\text{ref},b}$ is employed to lower the influence of such estimation. Intensity error estimation $C_{t,\text{ref},b}$ are finally weighted by the product of the two previous terms, giving equal influence to distance and reliability. In general it is possible to apply unequal weighting. If the distance term is favoured unreliable compensation values will degrade the quality of the restoration. If the influence of the distance term is diminished, blocking artefacts will emerge as shown in Figure 8. It has been experimentally observed that equal

FIGURE 7: Block-based partition of the first frame of *Boat* using a 3×3 grid. The pixel undergoing compensation and the centre of each block are represented by black and white dots, respectively. The black lines represent the Euclidean distances $c_b(p)$. Polynomial correction profiles $C_{t,\text{ref},b}$ and associated reliabilities $r_{t,\text{ref},b}$ are available for each block b. Compensation value for pixel $\vec{p}$ is obtainted by a bilinear interpolation of the block-based compensation values (9 in this example). Bilinear interpolation involves weighting by block-based reliabilities and distances d_b.

(a) (b)

FIGURE 8: (a) Compensation of the frame 20 of the test sequence *Boat* applied independently on each block of a 3×3 grid. As expected blocking artefacts are visible. (b) Compensation using the spatially adaptive version of the algorithm.

weights provide a good balance between the two. The final correction value is then given by

$$F_t'(\vec{p}) = F_t(\vec{p}) - \sum_{b=1}^{B} [d_b(\vec{p}) \cdot r_{t,\text{ref},b}(F_t(\vec{p}))] \cdot C_{t,\text{ref},b}(F_t(\vec{p})),$$
$$\text{with } \sum_{b=1}^{B} [d_b(\vec{p}) \cdot r_{t,\text{ref},b}(F_t(\vec{p}))] = 1. \tag{11}$$

Figure 7 illustrates the bilinear interpolation scheme. It shows block-partitioning, computed compensation profiles and reliabilities, and distances d_b. For pixel $\vec{p}$ the corresponding compensation value is given by bilinear interpolation of the block-based compensation values, weighted by their reliabilities and distances d_b.

4.2. Segmentation-based profile estimation

So far entire blocks have been considered for the compensation profile estimation. It was shown that the weighted polynomial fitting and the motion prediction are capable of dealing with outliers. However, it is also possible to enhance the robustness and the accuracy of the method by performing flicker estimation of regions of homogeneous brightness. The presence of outliers (Figure 5) is reduced in the compensation profile estimation and the compensation profile (Figure 6) is computed on a narrower grey-level range, improving the polynomial fitting accuracy.

In our approach we divide a degraded block into regions of uniform intensity and then perform one compensation profile estimation per region. Afterwards, the most reliable sections of the obtained profiles are combined to create a compound compensation profile. The popular unsupervised segmentation algorithm called JSeg [20] is used to partition the degraded image F_t into uniform regions (Figure 9). The method is fully automatic and operates in two stages. Firstly, grey-level quantisation is performed on a frame based on peer group filtering and vector quantisation. Secondly, spatial segmentation is carried out. A J-image where high and low values correspond to possible regions boundaries is created using a pixel-based so-called J measure. Region growing performed within a multi-scale framework allows to refine the segmentation map. For images sequence, a region tracking method is embedded into the region growing stage in order to achieve consistent segmentation. The choice

Table 3: Number of frames processed per second for the different compensation techniques.

	Proposed	Pitié [6]	Roosmalen [5]
352×288 resolution	0.62	0.80	0.55
720×576 resolution	0.35	0.43	0.27

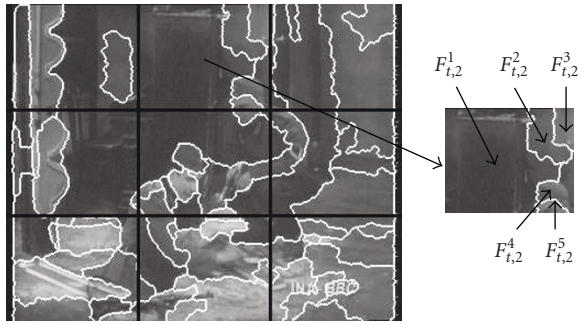

Figure 9: Segmentation and block-partitionning using a 3×3 grid of the 20th frame of the sequence *Tunnel*. Block partitioning ($B = 9$) and the overlaid segmentation map are presented on the left, while the right figure illustrates the segmentation of block $F_{t,2}$. Sub-regions $F^k_{t,2}$ ($k = 1, \ldots, 5$) where local compensation profiles are estimated are labelled.

of segmentation algorithm is not of particular importance. Alternative approaches such as Meanshift [21] or Statistical region merging [22] can also be employed for segmentation with similar results as the ones presented later in this paper.

The segmentation map is then overlaid onto the block grid, generating block-based subregions $F^k_{t,b}$, k being the index of the region within the block b. Block partitioning allows to deal with flicker spatial variability while grey-level segmentation permits to estimate flicker in uniform regions. Local compensation profiles $C^k_{t,\mathrm{ref},b}$ and associated reliabilities $r^k_{t,\mathrm{ref},b}$ are then computed independently on each subregion of each block. k compensation values are then available for each grey level and the aim is to retain the most accurate one. The quality of the region-based estimations is proportional to the frequency of occurrence of grey levels. Reliability measurement $r^k_{t,\mathrm{ref},b}$ presented in Section 3.2 is employed to reflect the quality of the region-based compensation values estimation. The block-based compensation value associated with grey-level I_t for block b is obtained by maximising the reliability $r^k_{t,\mathrm{ref},b}$ for the k region-based compensation values estimation:

$$\begin{aligned} C_{t,\mathrm{ref},b}(I_t) &= \max_{r^k_{t,\mathrm{ref},b}(I_t)} \{C^k_{t,\mathrm{ref},b}(I_t)\}, \\ r_{t,\mathrm{ref},b}(I_t) &= \max_k \{r^k_{t,\mathrm{ref},b}(I_t)\}. \end{aligned} \tag{12}$$

Finally, $\max_k \{r^k_{t,\mathrm{ref},b}(I_t)\}$ is retained as a measure of the block-based compensation value reliability.

5. FLICKER COMPENSATION FRAMEWORK

In this section, a new adaptive compensation framework achieving a dynamic update of the intensity error profile is presented. It is suitable for the compensation of long duration film sequences while it addresses problems arising from varying scene motion and illumination using a novel motion-compensation grey level tracing approach. Compensation accuracy is further enhanced by incorporating a block-based spatially adaptive model. Figure 10 presents a flow-chart describing the entire algorithm while Figure 2 shows the mean intensity of compensated frames between the baseline approach [7, 8] and the proposed algorithm. The baseline method relies on a reference frame (usually the first frame of the sequence) and is unable to cope with intentional brightness variations.

5.1. Adaptive estimation of the intensity error profile

The baseline compensation scheme described in [7] allows the correction of the degraded frame according to a fixed reference frame F_{ref} (typically the first frame of the shot). This is only useful for the restoration of static or nearly static sequences as performance deteriorates with progressively longer temporal distances between a compensated frame and the appointed reference especially when considerable levels of camera and scene motion are present. In addition it gives incorrect results if F_{ref} is degraded by other artefacts (scratches, blotches, special effects like fade-ins or even MPEG compression can damage a reference frame). Restoration of long sequences requires a carefully engineered compensation framework.

Let us denote by $C_{t,R}$ the intensity error profile between frame F_t and flicker-free frame F_R. We use an intuitively plausible assumption by considering that the average of intensity errors $C_{t,i}(I_t)$ between frames I_t and I_i within a temporal window centred at frame t yields an estimate of flicker-free grey-level I_R. Other assumptions could be formulated and median or polynomial filtering could be employed. The intensity error $C_{t,R}(I_t)$ between grey-levels I_t and I_R is estimated using the polynomial approximation $C_{t,i}(I_t)$ which provides a smooth and compact parametrisation of the correction profile (Section 3.2):

$$C_{t,R}(I_t) = \approx \frac{1}{N} \sum_{i=t-N/2}^{t+N/2} \Delta I_{t,i}(I_t). \tag{13}$$

In other words a correction value $C_{t,R}(I_t)$ on the profile is obtained by averaging correction values $C_{t,i}(I_t)$ where $i \in [t-N/2; t+N/2]$, that is, a sliding window of width N centred at the current frame. We incorporate reliability weighting (as obtained from Section 3.2) by taking into account individual reliability contributions for each frame within the sliding window which are normalised for unity:

$$C_{t,R}(I_t) = \sum_{i=t-N/2}^{t+N/2} r'_{t,i}(I_t) \cdot C_{t,i}(I_t) \quad \text{with} \quad \sum_{i=t-N/2}^{t+N/2} r'_{t,i}(I_t) = 1. \tag{14}$$

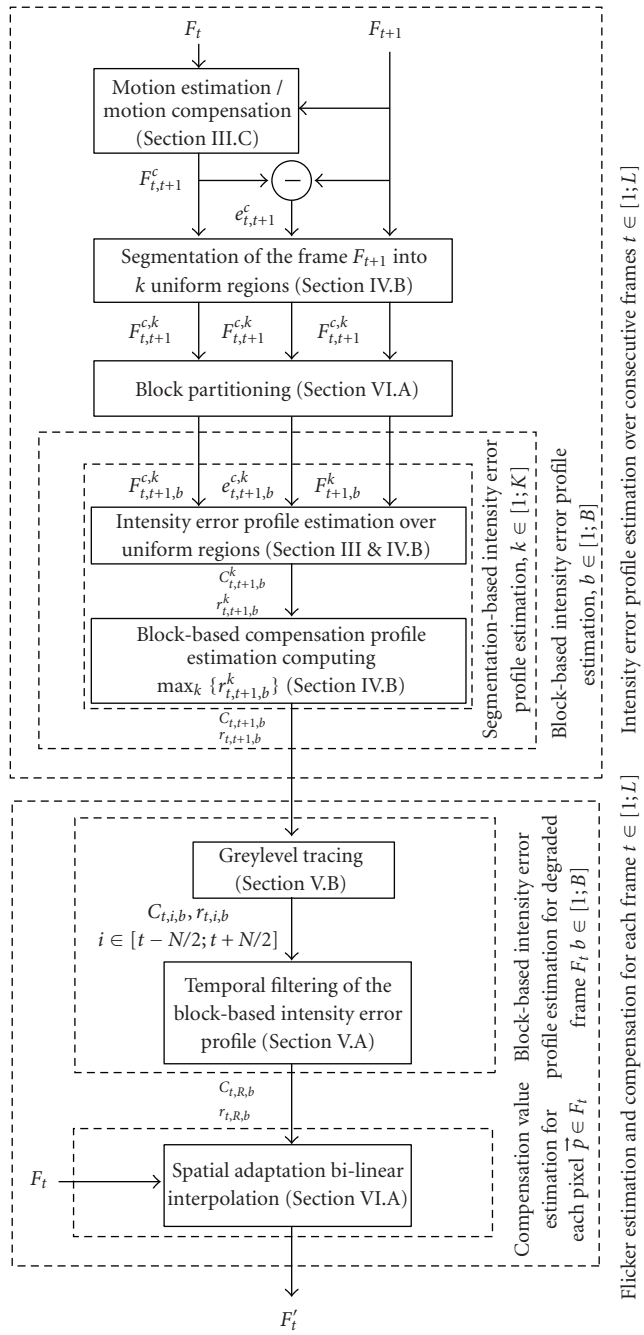

Figure 10: Flow chart of the proposed compensation algorithm. The algorithms operates in two stages: intensity error profile over consecutive frames are first computed on a block-based basis. Afterwards these profiles are employed to calculate block-based compensation profiles related to a specific degraded frame, which are finally bi-linearly interpolated to obtained pixels compensation values.

The scheme is summarised in the block diagram of Figure 11. A reliable correction value $C_{t,i}(I_t)$ will have a proportional contribution to the computation of $C_{t,R}(I_t)$. A reliability measure corresponding to $C_{t,R}(I_t)$ is obtained by summing unnormalised reliabilities $r_{t,i}(I_t)$ of interframe correction values $C_{t,i}(I_t)$ inside the sliding window:

$$r_{t,R}(I_t) = \sum_{i=t-N/2}^{t+N/2} r_{t,i}(I_t). \tag{15}$$

5.2. Intensity error estimation between distant frames using motion-compensated grey-level tracing

As Frames F_t and F_i can be distant in a film sequence, large motion may interfere and the motion compensation framework presented is Section 3.3 cannot be used directly as it is likely that the two distant frames are entirely different in terms of content. To overcome this we first estimate intensity error profile between motion-compensated consecutive

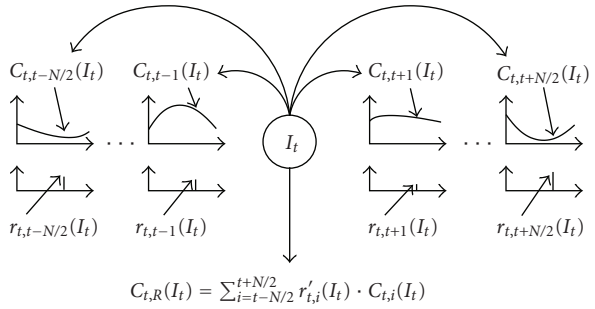

FIGURE 11: Compensation value $C_{t,R}(I_t)$ for a specific grey-level I_t is obtained by averaging inter-frame compensation values $C_{t,i}(I_t)$, $i \in [t - N/2; t + N/2]$ within a temporal window of width N centered at current frame F_t. Each inter-frame compensation value is weighted by its associated reliabilty $r_{t,i}(I_t)$.

frames. Raw intensity error profiles and associated reliabilities are computed between consecutive frames in both directions yielding values to $\Delta I_{t,t+1}, \Delta I_{t+1,t}$ and $r_{t,t+1}, r_{t+1,t}$ for $t = [0; L]$, L being the number of frames of the sequence (flow-chart 10, first stage). The mapping functions are then combined as follows:

$$\Delta I_{t,t+2}(I_t) = \Delta I_{t,t+1}(I_t) + \Delta I_{t+1,t+2}(I_t + \Delta I_{t,t+1}(I_t)) \quad (16)$$

which can be generalised for $\Delta I_{t,t\pm i}$, $i > 2$. This amounts to tracing correction values from one frame to the next along trajectories of estimated motion. The associated reliability is computed as follows:

$$r_{t,t+2}(I_t) = \min\left(r_{t,t+1}(I_t), r_{t+1,t+2}(I_t + \Delta I_{t,t+1}(I_t))\right). \quad (17)$$

The above generalises for any frame-pair (flow-chart 10, second stage). If a specific correction $\Delta I_{t,t\pm1}$ is unreliable then the min operator above ensures that the compound reliability $r_{t,t\pm i}(I_t)$ will also be rendered unreliable.

A numerical example is presented in Figure 12 where correction of grey-level 15 between frames F_t and F_{t+1} is estimated as $\Delta I_{t,t+1}(15) = -1$. Thus, grey-level 15 is mapped to grey-level 14 in F_{t+1}. As $\Delta I_{t+1,t+2}(14) = 2$ we have $\Delta I_{t,t+2}(15) = -1 + 2 = 1$. Nevertheless we know that $r_{t+1,t+2}(14) = 0.1$ which means that $\Delta I_{t+1,t+2}(14)$ is unreliable. As a consequence $\Delta I_{t,t+2}(15) = 1$ is not a trustworthy estimation and its reliability computed as $r_{t,t+2}(15) = \min(r_{t,t+1}(15), r_{t+1,t+2}(\Delta I_{t,t+1}(15))) = \min(0.9, r_{t+1,t+2}(14)) = \min(0.9, 0.1) = 0.1$ reflects that.

In the same manner we find that $\Delta I_{t,t+2}(20) = \Delta I_{t,t+1}(20) + \Delta I_{t+1,t+2}(\Delta I_{t,t+1}(20) + 20) = 5 + \Delta I_{t+1,t+2}(25) = 8$ and $r_{t,t+2}(20) = \min(r_{t,t+1}(20), r_{t+1,t+2}(\Delta I_{t,t+1}(20) + 20)) = \min(0.7, r_{t+1,t+2}(25)) = \min(0.7, 1) = 0.7$ which is more reliable than before.

6. EXPERIMENTAL RESULTS

6.1. Test material

The proposed flicker compensation framework is compared with two spatially-adaptive state-of-the-art techniques,

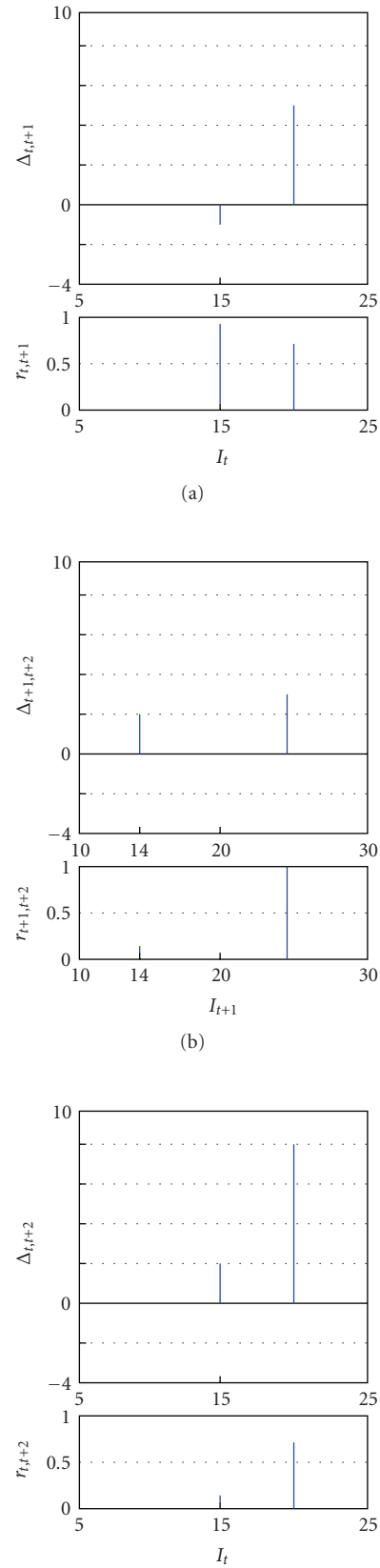

FIGURE 12: Example—Tracing of grey-levels 15 and 20 of frame t along frames $t + 1$ and $t + 2$. The evolution of reliability weights is also shown.

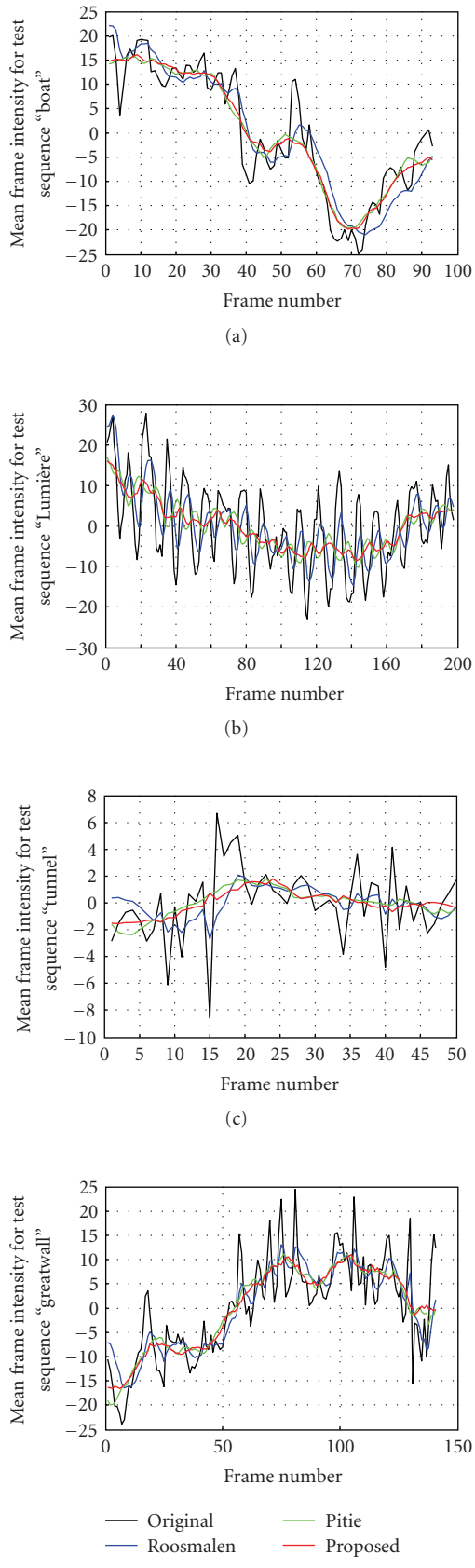

Figure 13: Comparison of mean frame intensity as a function of time.

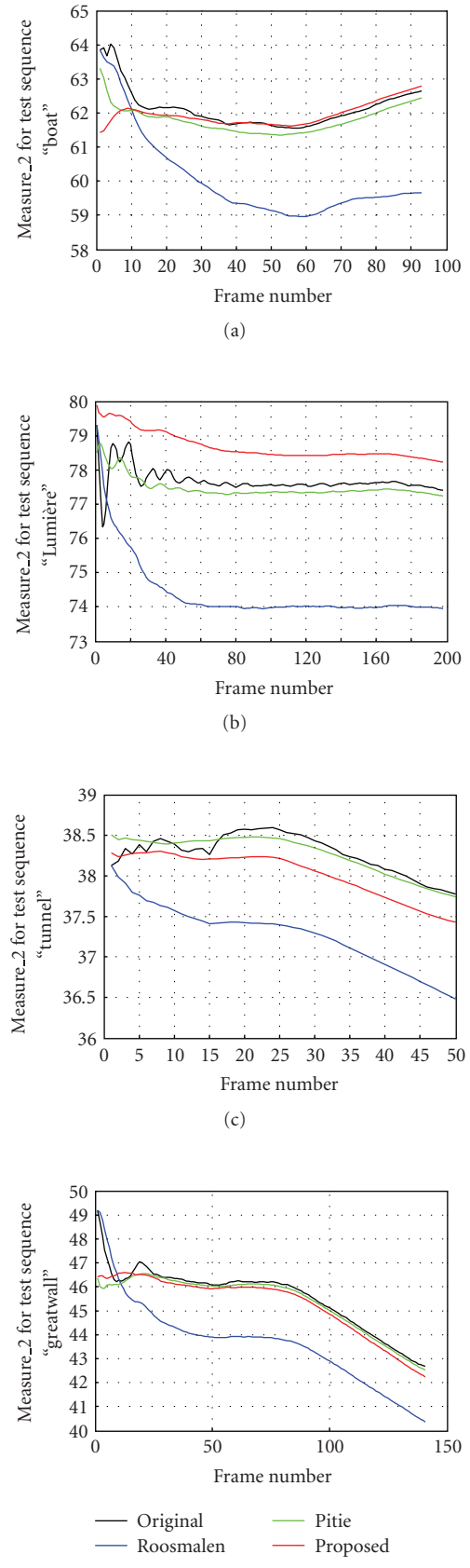

Figure 14: Comparison of time-normalised cumulative standard deviation.

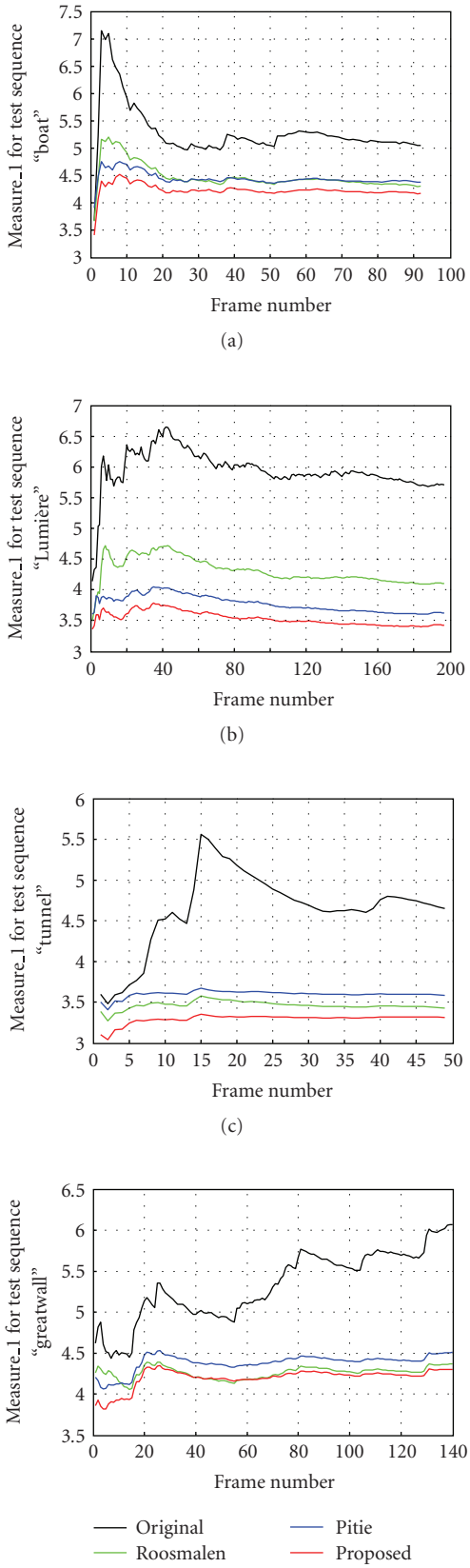

Figure 15: Comparison of time-normalised cumulative average of absolute differences between consecutive motion-compensated frames.

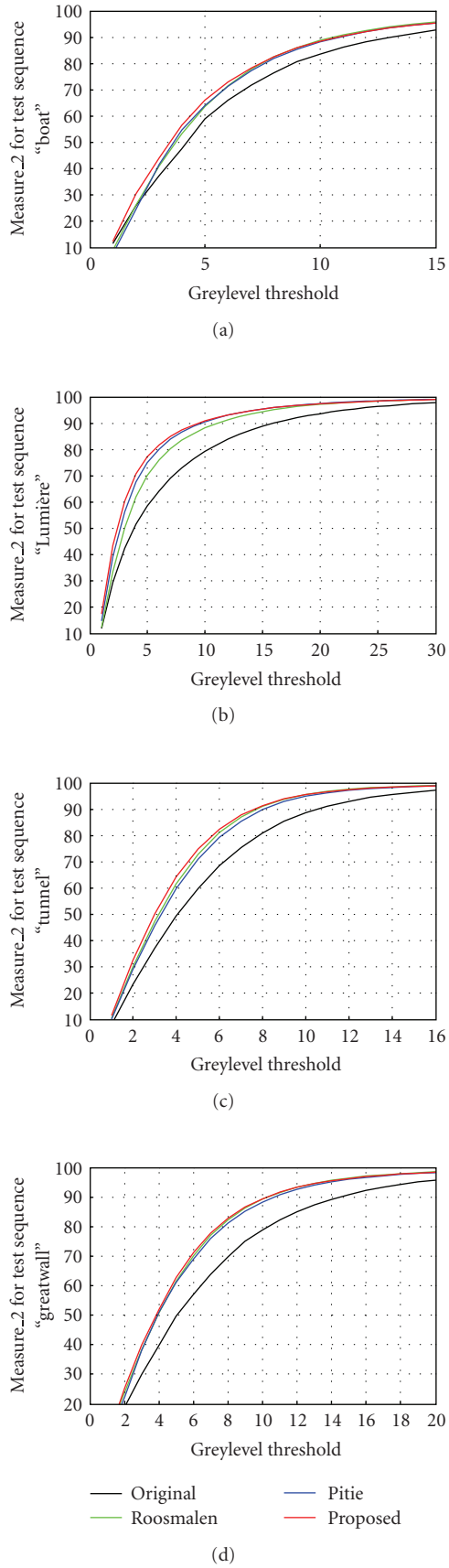

Figure 16: Comparison of percentage of motion-compensated pixels having an absolute difference lower than a variable threshold.

detailed, respectively, in [5, 6] (cf. Section 2). Four CIF resolution (360 × 288) monochromes test sequences, *Boat*, *Lumière*, *Tunnel* and *Greatwall* composed of 93, 198, 50 and 141 frames, respectively, are used for evaluation purposes. Each of these sequences represent historical footage and are therefore susceptible to other archive-related artefacts (such as dirt, unsteadiness and scratches) in addition to flicker.

The first three sequences contain slight unsteadiness but substantial levels of flicker. The impairments are highly nonlinear in and present various degrees of spatial variability. Motion content is quite low as the camera is fixed. The last sequence is a panoramic pan of the Chinese Great Wall.

6.2. Evaluation protocol

For each test sequence, a 4 × 4 grid-partitioning (cf. Section 4) is employed. In addition, the temporal window length (Section 5.1) is set to 15 frames centred at the current degraded frame. Flicker reduction algorithms are traditionally evaluated by examining the variation of the mean frame intensity over time. Those measurements are presented in Figure 13 for each of the test sequences. The smoother the curve, the better the compensation is supposed to be. It is also useful to compare the standard deviation of each frame as a good-quality compensation should not distort the greyscale dynamic range of the original frames. Time-normalised cumulative standard deviation of the frames for the available sequence are presented in Figure 14. Nevertheless these measurements cannot highlight the spatial variation issues discussed earlier in Section 1.1. Two new visualisation methods are proposed in order to highlight spatial variability. These provide flicker compensation objective measurements for sequences impaired by localised flicker and containing substantial scene motion.

Let us now consider a pair of flicker-compensated frames. In the case of a near-perfect correction, the first frame and the motion-compensated second one should be very similar, the differences being only due to motion estimation inaccuracy. The remaining two of the new visualisation techniques are based on this hypothesis and assess the similarity between those two images as follows.

(i) The absolute difference between co-sited pixels of the above frames is averaged. In addition this average is weighted for each pixel by considering the motion prediction error. The better the compensation, the closer to zero this value should be.

(ii) A threshold on the available greyscale (typically between 0 and 255) is applied. Then the percentage of co-sited pixels having an absolute difference lower than this threshold is counted. Each pixel's influence is weighted by the motion prediction error. A curve for the entire greyscale is then compiled by suitably moving the threshold across the scale.

The above are applied to image sequences by accumulating measurements obtained for pairs of consecutive frames. Normalising the values by the running total number of frames give mores clarity to the plots, which are, respectively, presented in Figures 15 and 16 for the seven test sequences under consideration.

6.3. Discussion

Overall, our results show that the three competing algorithms perform well both in terms of measured performances as well as subjective quality. Figure 13 demonstrates that a smoothing of frame mean intensity variation is achieved so the global flicker component is substantially reduced while temporal filtering (Section 5) allows to preserve natural brightness variation. It must be noticed that Roosmalen's curve is somehow more noisy than the two others for several test sequences and this is visually confirmed. Residual flicker is still visible, as the compensated frames are a mixture of the corrected and degraded ones (Section 2.3).

This performance difference is significantly more noticeable in Figure 14 where the time-normalised cumulative standard deviation of the frames are plotted. In terms of this criterion effective methods should reduce flicker while maintaining simultaneously the greyscale range of the test sequences. Pitié and the proposed method are able to preserve the dynamic range characteristics of the sequences, and increase it for test sequences *Boat* and *Lumière*. However, a dramatic reduction may be observed for Roosmalen's method. Comparing Pitié's technique to ours, we can see that each have a slight advantage for approximately half the test sequences. As mentioned previously, these measurements cannot highlight the flicker spatial variation issues. Next we assess performance in relation to spatial variability.

Better discrimination can be obtained by examining Figure 15, which shows the average variation between motion-compensated frames. It may be observed that the proposed technique compares favourably for all test sequences.

Finally the percentage of pixels having a lower absolute difference than a variable threshold between consecutive frames is computed in Figure 16. The higher the percentage the better the performance of the scheme under assessment. Also in this case our method performs best.

Test sequences and results obtained with the different approaches above are available at: http://www.ee.surrey.ac.uk/Personal/G.Forbin/EURASIP/index.html.

7. CONCLUSION

In this paper, a new scheme for flicker compensation was introduced. The approach was based on non-linear modelling introduced in previous work and contains important novel components such as flicker estimation on homogeneous regions and temporal filtering using grey-level tracing. These novelties allows to address, respectively, the challenges posed by the spatial variability of flicker impairments and the adaptive estimation of flicker compensation profile for long duration sequences and also scene motion. Our results demonstrate that the algorithm is very effective towards flicker compensation both in subjective and objective terms

and compares favourably to state-of-art methods that feature in the literature.

LIST OF SYMBOLS

F_t:	Frame sampled at time t
F'_t:	Flicker compensated frame sampled at time t
F_{ref}:	A generic reference frame
L:	Total number of frames in a test sequence
$\vec{p} = (x, y)$:	Pixel coordinates
$F_t(\vec{p})$:	Grey-level value of frame F_t at position $\vec{p}$
I:	Image intensity (grey-level value)
I_t:	Intensity I in frame F_t
$\Delta I_{t,\text{ref}}$:	Intensity error profile between frames F_{ref} and F_t
$\Delta I_{t,\text{ref}}(I_t)$:	Intensity error for grey-level I_t between frames F_{ref} and F_t
$r_{t,\text{ref}}$:	Intensity error reliability between frames F_{ref} and F_t
$r_{t,\text{ref}}(I_t)$:	Reliability associated with intensity error $\Delta I_{t,\text{ref}}(I_t)$
$P_{t,\text{ref}}$:	Polynomial fitted to intensity error profile between frames F_{ref} and F_t
$C_{t,\text{ref}}$:	Weighted polynomial fitted to intensity error profile between frames F_{ref} and F_t
$H_{t,\text{ref}}(I_t)$:	Histogram of the intensity errors between pixels with intensity I_t in frame F_{ref} and co-sited pixels in frame F_t
$F^c_{t,\text{ref}}$:	Motion-compensated version of F_{ref} relative to F_t
$e^c_{t,\text{ref}}$:	Motion prediction error of $F^c_{t,\text{ref}}$
$E^c_{t,\text{ref}}$:	Error weighting derived from $H^c_{t,\text{ref}}(I_t)$
$H^c_{t,\text{ref}}(I_t)$:	Histogram of the intensity errors between pixels with intensity I_t in frame F_t and co-sited pixels in
B:	Number of blocks considered in the block partitioning scheme
$C_{t,\text{ref},b}$:	Intensity error profile computed within block b between frames F_{ref} and F_t
$r_{t,\text{ref},b}$:	Reliability associated with intensity error $C_{t,\text{ref},b}$
$C^k_{t,\text{ref},b}$:	Intensity error profile computed within region k between blocks $F_{\text{ref},b}$ and $F_{t,b}$
$r^k_{t,\text{ref},b}$:	Reliability associated with intensity error $C^k_{t,\text{ref},b}$
$d_b(\vec{p})$:	Inverse of euclidean distance between position $\vec{p}$ and centre of block b
N:	Number of frames in the temporal filtering window
F_R:	Flicker-free frame F_t
I_R:	Flicker-free intensity I_t
$C_{t,R}$:	Intensity error profile between flicker-free frames F_R and F_t
$r_{t,R}$:	Reliability associated with intensity error $C_{t,R}(I_t)$.

ACKNOWLEDGMENT

This work was supported by the UK Engineering and Physical Sciences Research Council (EPSRC) under Research Grant GR/S70098/01.

REFERENCES

[1] Y. Wu and D. Suter, "Historical film processing," in *Applications of Digital Image Processing XVIII*, vol. 2564 of *Proceedings of SPIE*, pp. 289–300, San Diego, Calif, USA, July 1995.

[2] E. Decencière Ferrandière, *Restauration automatique de films anciens*, Ph.D. dissertation, Ecole Nationale Supérieure des Mines de Paris (ENSMP), Paris, France, 1997.

[3] P. Richardson and D. Suter, "Restoration of historic film for digital compression: a case study," in *Proceedings of IEEE International Conference on Image Processing (ICIP '95)*, vol. 2, pp. 49–52, Washington, DC, USA, October 1995.

[4] V. Naranjo and A. Albiol, "Flicker reduction in old films," in *Proceedings of IEEE International Conference on Image Processing (ICIP '00)*, vol. 2, pp. 657–659, Vancouver, Canada, September 2000.

[5] P. M. B. van Roosmalen, R. L. Lagendijk, and J. Biemond, "Correction of intensity flicker in old film sequences," *IEEE Transactions on Circuits and Systems for Video Technology*, vol. 9, no. 7, pp. 1013–1019, 1999.

[6] F. Pitié, R. Dahyot, F. Kelly, and A. C. Kokaram, "A new robust technique for stabilizing brightness fluctuations in image sequences," in *Proceedings of the ECCV Workshop on Statistical Methods in Video Processing (ECCV-SMVP '04)*, vol. 3247, pp. 153–164, Prague, Czech Republic, May 2004.

[7] T. Vlachos, "Flicker correction for archived film sequences using a nonlinear model," *IEEE Transactions on Circuits and Systems for Video Technology*, vol. 14, no. 4, pp. 508–516, 2004.

[8] G. Forbin, T. Vlachos, and S. Tredwell, "Spatially adaptive flicker compensation for archived film sequences using a nonlinear model," in *Proceedings of the 2nd IEE European Conference on Visual Media Production (CVMP '05)*, pp. 241–250, London, UK, November-December 2005.

[9] P. Schallauer, A. Pinz, and W. Haas, "Automatic restoration algorithms for 35 mm film," *Videre*, vol. 1, no. 3, pp. 60–85, 1999.

[10] T. Ohuchi, T. Seto, T. Komatsu, and T. Saito, "A robust method of image flicker correction for heavily-corrupted old film sequences," in *Proceedings of IEEE International Conference on Image Processing (ICIP '00)*, vol. 2, pp. 672–675, Vancouver, Canada, September 2000.

[11] A. C. Kokaram, R. Dahyot, F. Pitié, and H. Denman, "Simultaneous luminance and position stabilization for film and video," in *Image and Video Communications and Processing*, vol. 5022 of *Proceedings of SPIE*, pp. 688–699, Santa Clara, Calif, USA, January 2003.

[12] S. Stigler, *The History of Statistics*, Belknap Press of Harvard University Press, Cambridge, Mass, USA, 1986.

[13] F. Galton, "Regression towards mediocrity in hereditary stature," *Journal of the Anthropological Institute*, vol. 15, pp. 246–263, 1886.

[14] F. Pitié, B. Kent, B. Collis, and A. C. Kokaram, "Localised deflicker of moving images," in *Proceedings of the 3rd IEE European Conference on Visual Media Production (CVMP '06)*, pp. 134–143, London, UK, November 2006.

[15] J. Jung, M. Antonini, and M. Barlaud, "Automatic restoration of old movies with an object oriented approach," in *Proceedings of the French Conference on Pattern Recognition and Artificial Intelligence (RFIA '00)*, pp. 557–565, Paris, France, February 2000.

[16] J. Delon, "Movie and video scale-time equalization application to flicker reduction," *IEEE Transactions on Image Processing*, vol. 15, no. 1, pp. 241–248, 2006.

[17] C. Mess, *The Theory of the Photographic Process*, McMillan, New York, NY, USA, 1954.

[18] P. J. Huber, *Robust Statistics*, John Wiley & Sons, New York, NY, USA, 1981.

[19] M. J. Black and P. Anandan, "The robust estimation of multiple motions: parametric and piecewise-smooth flow fields," *Computer Vision and Image Understanding*, vol. 63, no. 1, pp. 75–104, 1996.

[20] Y. Deng and B. S. Manjunath, "Unsupervised segmentation of color-texture regions in images and video," *IEEE Transactions on Pattern Analysis and Machine Intelligence*, vol. 23, no. 8, pp. 800–810, 2001.

[21] D. Comaniciu and P. Meer, "Mean shift: a robust approach toward feature space analysis," *IEEE Transactions on Pattern Analysis and Machine Intelligence*, vol. 24, no. 5, pp. 603–619, 2002.

[22] R. Nock and F. Nielsen, "Statistical region merging," *IEEE Transactions on Pattern Analysis and Machine Intelligence*, vol. 26, no. 11, pp. 1452–1458, 2004.